Electrical properties and defect chemistry of anatase (TiO2)

Alicia Weibel, Renaud Bouchet, Philippe Knauth

Electrical properties and defect chemistry of anatase (TiO_2)

A. Weibel, R. Bouchet and P. Knauth

MADIREL, Université de Provence-CNRS (UMR 6121), Centre St Jérôme, 13397 Marseille Cedex 20, France

Abstract

The electrical properties of pure Anatase are investigated by impedance spectroscopy as function of temperature and oxygen partial pressure. The experimental results are fully interpreted by point defect chemistry. A transition from predominant Schottky to Frenkel cation disorder is observed when the temperature increases and/or the oxygen partial pressure decreases. The reduction enthalpies are near those obtained for Rutile in previous studies.

Keywords: Ceramic; Microstructure; Impedance spectroscopy; Point defects

1. Introduction

Titanium dioxide TiO_2 is one of the most important binary oxides for technological applications. Besides its well-known use as ubiquitous white pigment, it is also currently under investigation for high added-value environmental applications, including photocatalysis [1] and photoelectrochemical cells [2]. Photo-activity of TiO_2 is strongly correlated to the structure and microstructure of the powder. Titanium dioxide can present several crystalline structures: the most important are Rutile, Anatase and Brookite. Whereas the Rutile phase is clearly the thermodynamically stable one at high temperature, Anatase and Brookite can be obtained at reduced temperature; their metastability is strongly correlated to the surface composition of the oxide, and, thus, to the preparation conditions. For example, the so-called "sulphate route" is known to stabilize the Anatase phase, whereas the "chloride route" is more favourable for the formation of Rutile [3]. Moreover, particle size can have a strong impact on thermodynamic stability of the TiO_2 polymorphs; according to Ranade et al. [4], Anatase and Brookite, which have lower surface enthalpies than Rutile, are stable at small particle size. The electrical properties of titanium dioxide were mostly investigated for the Rutile modification as single crystals [5], [6], [7] and [8], microcrystalline materials [9], [10] and [11] at high temperature and, more recently, in nanocrystalline form [12]. At low oxygen partial pressures $P(O_2)$, Rutile shows generally n-type electronic conductivity, due to a large oxygen deficiency (TiO_{2-x}: $x \approx 10^{-3}$ at T = 800 °C and $P = 10^{-16}$ Pa [10]). Rutile can be readily doped and p-type or mixed ionic–electronic conduction have been reported occasionally in the high $P(O_2)$ domain [13], but discrepancies remain concerning the ionic contribution and the literature results are controversial. Baumard and Tani [14] determined an ionic transference number of only 10^{-3} at 1000 °C. At 1000 °C and $P(O_2) = 10^5$ Pa, Carpentier et al. [15] found an ionic transference number below 0.05 and Cronemeyer [16], a negligible ionic contribution. In contrary, Nowotny et al. [5] measured between 700 and 1100 °C in an oxygen partial pressure range 1–10^5 Pa an ionic transference number of 0.5 with an activation energy of 1.6 eV for the ionic conductivity. Popov et al. [17] reported ionic conduction below 1000 °C with an activation energy between 0.55 and 0.75 eV along *c* axis and 2 eV along *a* axis. Finally, Singheiser and Auer [18] estimated that ionic conduction plays an important role even in reduced TiO_2 (10^{-14}–10^{-19} Pa) between 900 and 1000 °C, but did not give numbers.

Fundamental studies on the electrical properties of the Anatase modification are seldom, given that ceramic preparation and long-time measurements at elevated temperature generally lead to a grain growth and a partial phase transition into rutile. Knauth and Tuller studied the electrical properties of dense nanocrystalline Anatase as function of temperature and oxygen partial pressure [19]. Porous Anatase ceramics were investigated by Azad et al. [20] in view of gas (CO and H_2) sensor applications. Studies of dense nanocrystalline ceramics were also performed by Bhowmik et al. [21], but here the material was a two-phase Anatase–Rutile mixture. Finally, an influence of humidity was shown [22]. To make a long story short: there is a clear interest in electrical properties of Anatase, but experimental problems are numerous and therefore the literature data are rare and partly controversial.

This study reports *ac* electrical measurements of dense, phase-pure Anatase ceramics over the largest oxygen partial pressure range ever investigated. In order to succeed, a certain number of difficult problems had to be solved. First, dense phase-pure Anatase ceramics had to be processed from nanometric precursor powders; this is not possible by conventional high temperature sintering. Second, the electrical measurements had to be made at relatively low temperatures in order to keep the Anatase structure and avoid grain growth. These experiments demanded to optimize the usual procedure in order to cope with the difficult equilibration of the oxide with the surrounding gas phase at reduced temperature.

2. Experimental

2.1. Anatase powders

The Anatase powders were prepared by the sulfate route [23]. In this process, the mineral precursor was dissolved in sulfuric acid and the titanium sulfate solution then hydrolyzed by heating to 95–110 °C. The hydrolysis product was filtered and the filtrate thoroughly washed until neutral pH was obtained. It was then calcined under air for 1 h at a temperature between 300 and 1100 °C to obtain a well-defined particle size distribution; phase-pure samples calcined at 800 °C with a grain size of (70 ± 35) nm were used in the following [24]. The obtained powders were chemically analyzed by gravimetric techniques and ICP emission analysis. The concentrations of various impurities are given in Table 1 (total impurity content ≈ 0.25 mol%).

Table 1.

Impurity content (ppm) in anatase precursor powders (Gravimetric and ICP analysis)

Element	**Concentration/ppm**	
	ICP	Gravimetry
Na	930	1200–1300
Si	200	385
S	410	270
Other: P 270, Zr 175, Nb 68, Mg 21, Al 13, V 9, Fe 8, Pb 5, Ba 4, Cr 3, Zn 3, Cu 2, Ni, Co, Mn < 1		

2.2. Ceramic processing

Nanocrystalline Anatase ceramics were made by hot-pressing the powders calcined at 800 °C. In this procedure, the powder was introduced in pure alumina dies, cold compacted at 0.2 GPa and then uniaxially compressed under 0.44 GPa and subjected to a fixed heating rate of 5 °C/min up to a plateau temperature of 585 °C, where it was kept for 2 h, before releasing pressure and cooling with the intrinsic cooling rate of the hot-press (Cyberstar, Grenoble). The density of the nanocrystalline ceramics was determined from mass and geometrical dimensions. Densities of (91 ± 2)% of theory, based on the density of pure Anatase, were obtained under these conditions [25]. Microstructure and grain size of ceramics were determined both by Scanning Electron Microscopy (SEM) and Transmission Electron Microscopy (TEM) micrograph analysis. SEM experiments (Philips XL30 SFEG) were carried out on a chip of ceramic in secondary electron mode at 10–15 kV acceleration voltage. TEM experiments (JEOL 2010 F) were realized at 200 kV on a 15 × 5 × 0.1 μm thin blade obtained by Focused Ion Beam (Philips FIB 200) cutting (CP2M, Marseille). Finally, the samples were investigated by X-ray diffraction (Siemens D 5000) to check the absence of Rutile phase after hot-pressing and again after conductivity measurements.

2.3. Oxygen pump-sensor

The experimental set-up, schematically shown in Fig. 1, was described previously [26]. Briefly, it contains 4 high purity gas bottles (Ar, O_2, CO_2 and 10% H_2 in Ar from Air Liquide, France), which are connected to mass flowmeters to control gas mixtures and flux. Then, gas mixtures are led through the electrochemical oxygen pump (held at 900 °C), the potentiometric oxygen sensor and finally reach the experimental cell described by Steil [27] where the ceramics are equilibrated with the gas. The oxygen sensor and the ceramics are

maintained at the same temperature to measure the real oxygen partial pressure in contact with the sample especially at low temperature.

Fig. 1. Oxygen pump-sensor cell.

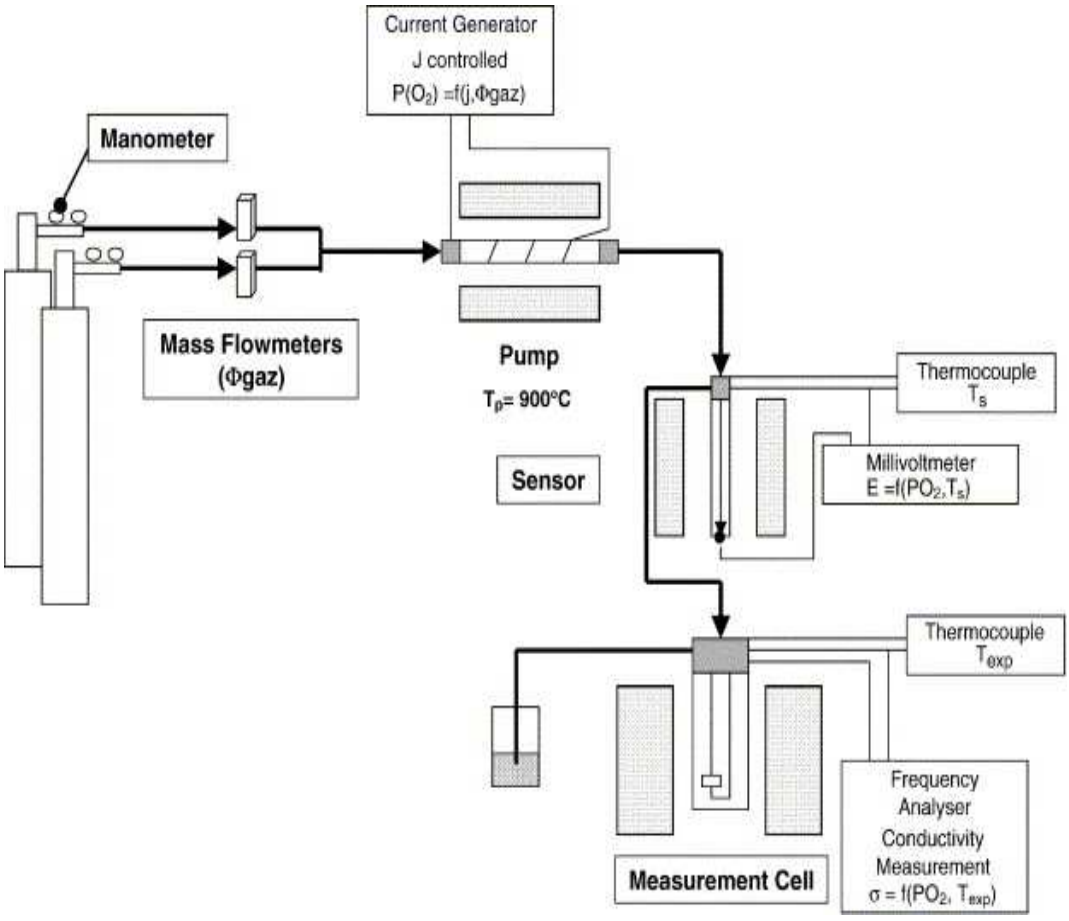

Different oxygen partial pressure domains can be accessed depending on the initial gas mixture and temperature used [28]. Between 450 and 700 °C, oxygen partial pressures between $5\ 10^{-9}$– $5\ 10^{-19}$ Pa can be obtained by reduction of CO_2 following the reaction:

$$CO_2 = CO + 1 / 2\ O_2. \quad (1)$$

The standard free enthalpy of (1) is: $\Delta G°(T) = 283.328 - 0.08753\ T$ (/ kJ mol^{-1}) [28]. However, according to Ellingham diagrams, strong reduction of CO_2 into CO at these

temperatures can lead to parasitic CO reduction into carbon, following the Boudouard reaction:

$$2\ CO = C(s) + CO_2. \quad (2)$$

The absence of carbon was periodically checked in our experiments.

In the same temperature range, the lowest $P(O_2)$ domain, 10^{-15}– 10^{-25} Pa, is accessible by hydrogen oxidation:

$$H_2 + 1 / 2\ O_2 = H_2O. \quad (3)$$

The standard free enthalpy of reaction (3) is: $\Delta G°(T) = -247.657 + 0.0552\ T$ (/ kJ mol^{-1}) [28].

Finally, the high $P(O_2)$ range (10^5– 10^{-1} Pa) is obtained starting from oxygen–argon mixtures.

The measurement temperature was below 700 °C in order to keep the Anatase structure and to avoid grain growth.

Measurement campaigns were always realized from oxidizing to reducing conditions, starting with pure oxygen ($P(O_2) = 10^5$ Pa) and going to the most reducing H_2/H_2O mixture ($P(O_2) \approx 10^{-24}$ Pa). Reproducibility was checked after a complete run at maximum temperature (700 °C) to confirm the absence of major sample modifications, by grain growth or phase transition.

2.4. Impedance spectroscopy

Impedance measurements were made at open circuit potential in a frequency domain between 10^{-1} and 3×10^7 Hz using a frequency response analyzer Solartron SI 1260. Three samples could be studied at the same time. Reproducibility of our results was checked on two pellets. The signal amplitude was optimized in each experiment in order to maintain a linear response with the best quality spectrum. Sputtered gold or platinum electrodes with approximate thickness 200 nm were used to analyze the electrode reaction, but they gave comparable results at high $P(O_2)$. The signal stabilization after change of oxygen partial pressure took between 2 and 5 h.

3. Results

Two characteristic micrographs of Anatase ceramics are presented in Fig. 2a (SEM) and 2b (TEM). The observation of particles larger than 100 nm in the last case is unlikely due to the low probability of cutting the big particles in the center. The image analysis shows an average grain size and a grain size distribution similar to that of the precursor powder (Fig. 2c) of about (70 ± 35) nm [24]. The crystalline growth is negligible during hot-pressing, because the sintering temperature (585 °C) was below the calcination temperature of the initial powder (800 °C). The residual porosity is confirmed to be low and the pore size seems to be inferior to 5 nm (Fig. 2b). The high resolution micrograph shown in Fig. 2d and centred on grain interfaces, is characteristic of grain boundaries without precipitated crystalline or vitreous phases, which is confirmed by the zoom (Fig. 2e) of Fig. 2d. Fig. 3 presents the corresponding X-ray diffraction pattern for the powder precursor (a) and the ceramic after 700 °C electrical measurements (b): there are no peaks corresponding to the Rutile phase but the peaks appear slightly thinner indicating a very small increase of grain size.

Fig. 2. (a) is the SEM micrograph and (b) is the TEM micrograph of dense anatase ceramic, (c) TEM micrograph of precursor powder calcined at 800 °C for 1 h, (d) High Resolution micrograph centred on grain interfaces and (e) Zoom (white square) of (d).

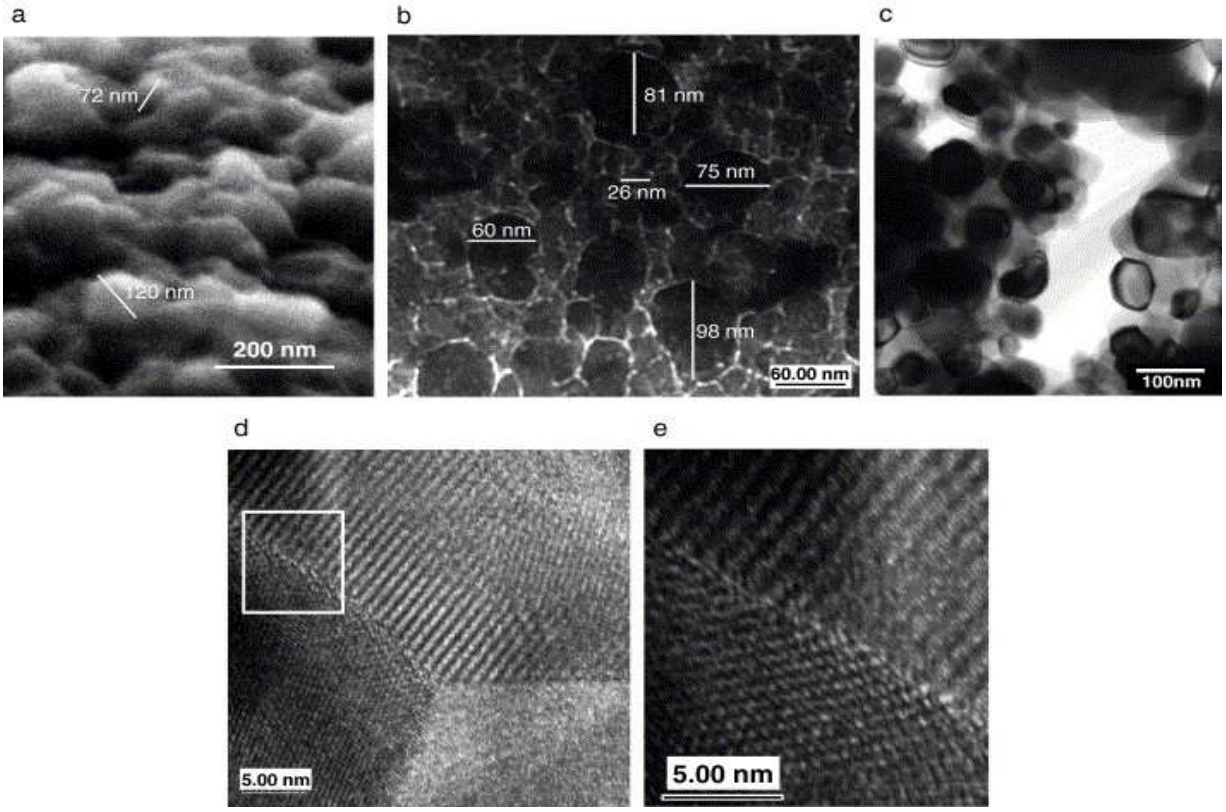

Fig. 3. X-ray diffraction patterns of a) starting powder calcined at 800 °C for 1 h and b) a dense phase-pure anatase ceramic obtained. The dashed lines represent the most intense diffraction lines of the rutile phase.

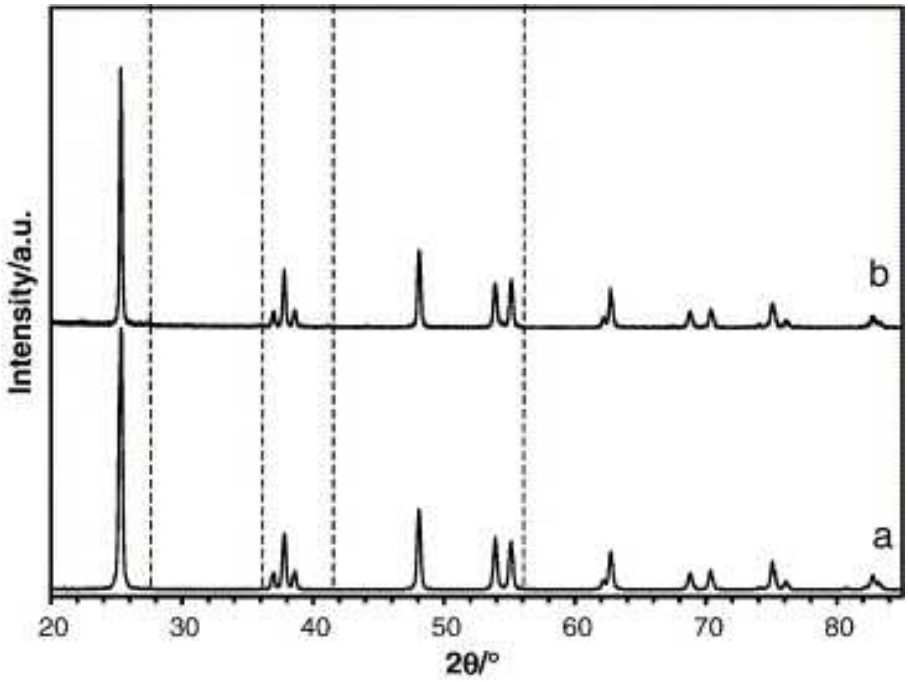

Typical impedance diagrams of Anatase ceramics are shown in Nyquist representation at high $P(O_2) = 10^5$ Pa as function of temperature in Fig. 4a–b and at 701 °C as function of $P(O_2)$ in Fig. 4c–d. Under pure oxygen, one notices at high frequencies a depressed arc followed by a not well-defined arc at low frequencies. This last contribution attributable to electrode reaction progressively decreases as the temperature increases and it disappears when the oxygen partial pressure decreases, i. e. below 100 Pa of O_2. Furthermore, sputtered platinum or gold electrodes gave similar results. This indicates that the Anatase ceramics are mostly electronic conducting with a negligible ionic conductivity at high oxygen partial pressure and low temperature. Coming back to the material response, at high $P(O_2)$, the observed depressed arc at high frequency can be interpreted with the classical series circuit of two parallel resistance-constant phase elements (CPE). At $P(O_2)$ below 1 Pa, the circuit can be simplified using only one parallel resistance-constant phase elements (CPE) and at $P(O_2)$ below 10^{-18} Pa (at 501 °C) or below 10^{-8} Pa (at 701 °C) a simple inductance in series with a resistance is used (Fig. 4e). The inductive element at high frequency is representative of the electrical connections. These spectra clearly indicate the electronic nature of the Anatase conductivity.

To compare data over the entire $P(O_2)$ range, we use the total high frequency resistance for conductivity calculations.

Fig. 4. Typical impedance diagrams in Nyquist representation of Anatase ceramics a) and b) at 10^5 Pa as a function of temperature, c) and d) at 701 °C as a function of $P(O_2)$ and e) the equivalent circuits used.

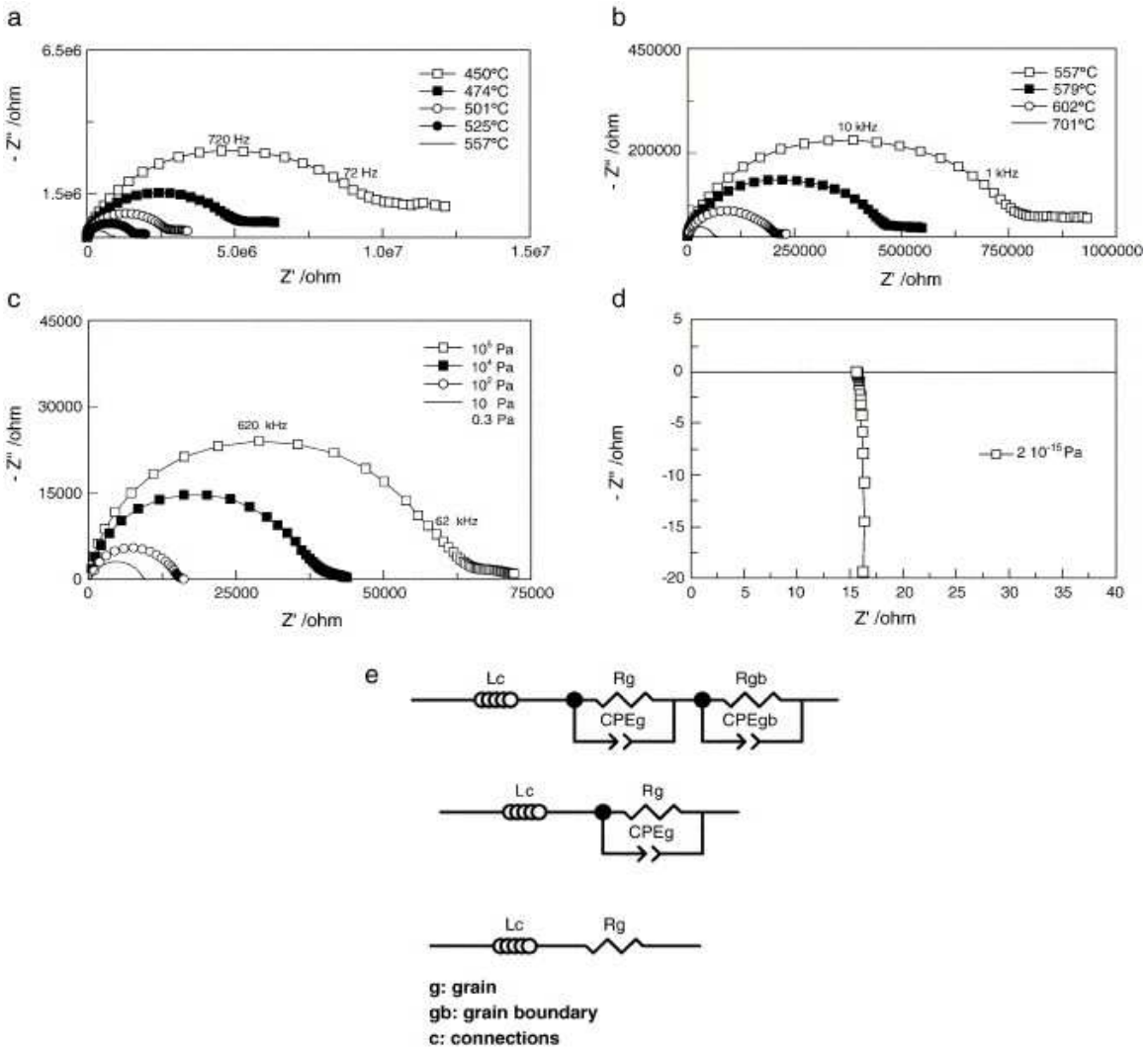

The electrical conductivity of Anatase is plotted in a double-logarithmic plot versus oxygen partial pressure in Fig. 5. Over more than 30 decades of $P(O_2)$, one notices linear dependencies, but the pressure dependence is not identical and the slope is lower below 579 °C (− 1 / 6) than above 650 °C (− 1 / 5). For example, at 579 and 701 °C, we determined by linear regression slope values of − 0.1631 and − 0.1957, very close to − 1 / 6 and − 1 / 5 and with very satisfactory correlation coefficients (0.9983 and 0.9988, respectively).

Fig. 5. Oxygen partial pressure dependence of electrical conductivity for Anatase TiO_2 between 450 and 701 °C.

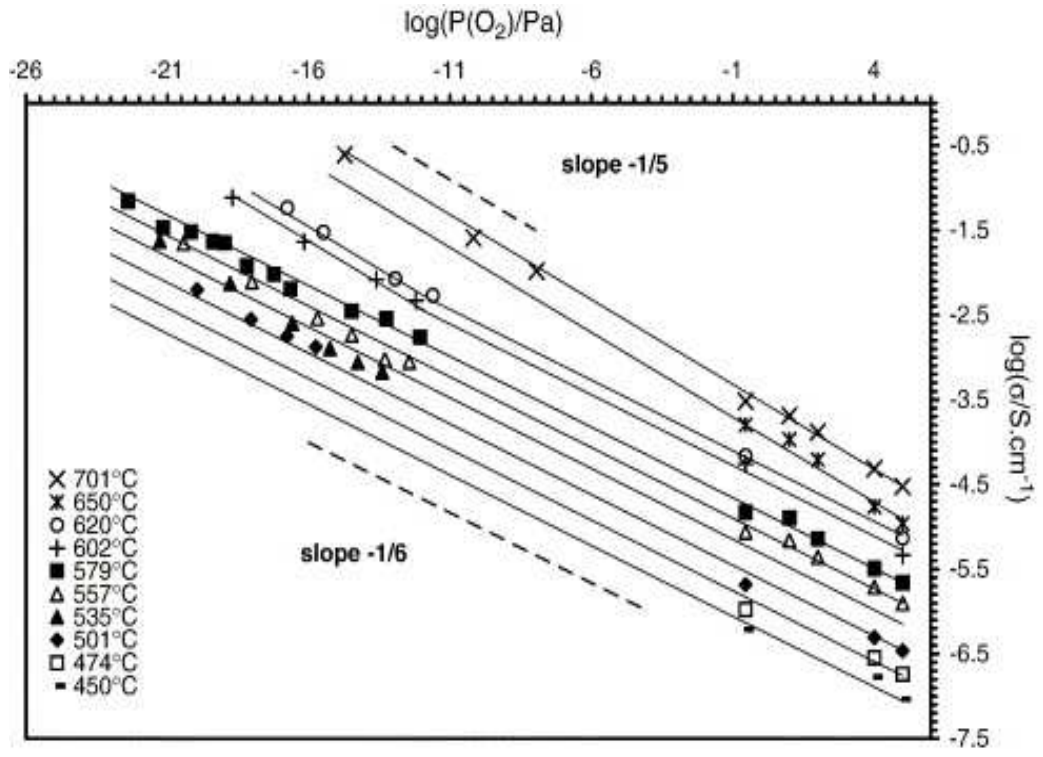

The temperature dependence is shown in Arrhenius representation under different oxygen partial pressures in Fig. 6. A unique straight line is observed at high oxygen partial pressures, but a change of slope, reflecting an activation energy change, is evident under low $P(O_2)$ at a temperature above 600 °C. Moreover, the slope change in Fig. 6 is correlated to variation of slope in Fig. 5.

Fig. 6. Arrhenius plot of electrical conductivity for Anatase TiO_2 under oxygen partial pressures of 10^{-15} and 10^{5} Pa.

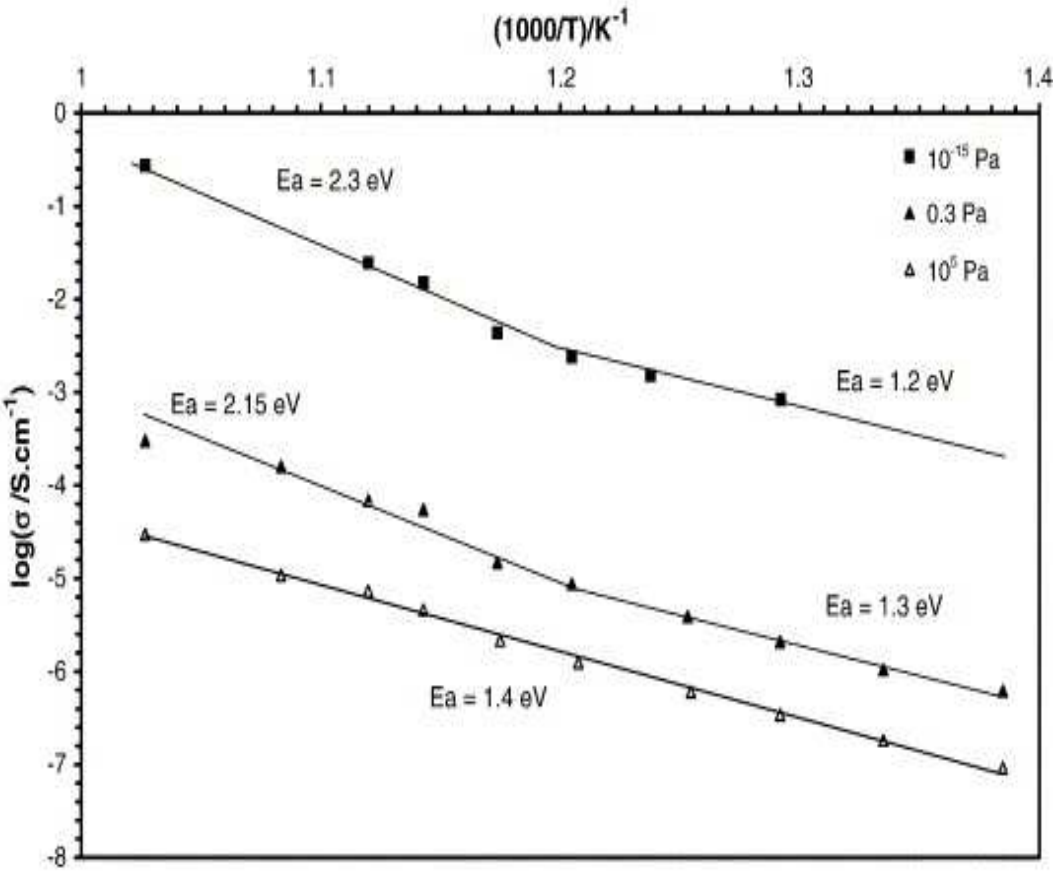

4. Discussion

The observed partial pressure and temperature dependencies indicate a change of defect reaction and can be nicely interpreted by point defect chemistry.

4.1. Intrinsic ionic and electronic defect equilibria

There are contradictions in literature on the disorder type in titanium dioxide, with reports of either Schottky or Frenkel cation type. The respective defect chemical reactions are written in Kröger nomenclature [29]:

Schottky disorder:

$$Ti_{Ti} + 2\ O_O = V_{Ti}^{4'} + 2\ V_O^{2\bullet} + TiO_2 \quad (4)$$

$$K_S = [V_{Ti}^{4'}]\ [V_O^{2\bullet}\}] = \exp(-\Delta\ G_S^{\ 0} / RT) \quad (5)$$

Frenkel cation disorder:

$$Ti_{Ti} + V_i = Ti_i^{4\bullet} + V_{Ti}^{4'} \quad (6)$$

$$K_F = [V_{Ti}^{4'}]\ [Ti_i^{4\bullet}] = \exp(-\ \Delta G_F^\circ / RT). \quad (7)$$

In the equilibrium constants K_S and K_F, the brackets represent the molar fractions of point defects and ΔG° is the standard free enthalpy of the corresponding defect reaction. Fully ionized defects can be assumed, because the ionization energies are relatively small in TiO_2 [9].

The intrinsic formation of electronic defects can be written:

$$0 = h^{\bullet} + e' \quad (8)$$

$$K_e = p\ n = Nc\ Nv \exp\ (-\ E_g / RT) \quad (9)$$

h• and e′ represent an electron hole and an excess electron with respective concentrations p and n; Nc and Nv are the density of states and E_g the band gap energy, which depends on particle size [30]. Reddy et al. reported for anatase structure an average value: $E_g = (3.3 \pm 0.1)$ eV [30].

4.2. Extrinsic disorder: non-stoichiometry

The reduction of TiO_2 at low oxygen partial pressures can be described by different reactions, depending on the assumed predominant disorder type (Schottky or cation Frenkel). For predominant Schottky disorder, the reduction reaction involves formation of oxygen vacancies $V_O^{2\bullet}$:

$$O_O = V_O^{2\bullet} + 2\ e' + 1 / 2\ O_2(g) \quad (10)$$

$$K_{Vo}^{2\bullet} = [V_O^{2\bullet}]\ n^2\ p(O_2)^{1/2} = \exp(-\ \Delta G^\circ_{red\ VO}{}^{2\bullet} / RT) \quad (11)$$

$\Delta G°_{red\ VO}{}^{2\bullet}$ is the standard Gibbs free enthalpy of reduction of TiO_2 with formation of oxygen vacancies. Using Brouwer's approximation for the electroneutrality condition, $n = 2\,[V_O{}^{2\bullet}]$, one obtains:

$$n^3 = 2\,K_{Vo}{}^{2\bullet}\,p(O_2)^{-1/2} \tag{12}$$

$$n = 2^{1/3}\exp(-\Delta G°_{red\ VO}{}^{2\bullet}/3RT)\,p(O_2)^{-1/6}. \tag{13}$$

For predominant Frenkel cation disorder, the reduction reaction involves titanium interstitials $Ti_i{}^{4\bullet}$. Only fully ionized titanium interstitials are considered, given the low ionization energies [31]:

$$Ti_{Ti} + 2\,O_O = Ti_i{}^{4\bullet} + 4\,e' + O_2\,(g) \tag{14}$$

$$K_{Ti\,i}{}^{4\bullet} = [Ti_i{}^{4\bullet}]\,n^4\,p(O_2) = \exp(-\Delta G°_{red\ Ti\,i}{}^{4\bullet}/RT) \tag{15}$$

$\Delta G_{red}°\ Ti_i{}^{4\bullet}$ is the standard Gibbs free enthalpy of reduction with titanium interstitial formation. Using the Brouwer approximation, $n = 4\,[Ti_i{}^{4\bullet}]$, one can write:

$$n = 4^{1/5}\exp(-\Delta G°_{red\ Ti\,i}{}^{4\bullet}/5RT)\,p(O_2)^{-1/5} \tag{16}$$

4.3. Conductivity data below 580 °C: $\sigma\ \alpha\ P(O_2)^{-1/6}$

The total conductivity of a solid can be written as the sum of electronic and ionic contributions:

$$\sigma = F(\mu_h p + \mu_e n + \Sigma_i \mu_i z_i [i]) \tag{17}$$

μ is the charge carrier mobility. Under reducing conditions, the electronic conductivity is much larger and the other contributions can be neglected. In this domain, conductivity can be expressed using Eqs. (13) and (17) and the Gibbs–Helmholtz equation $\Delta G° = \Delta H° - T\,\Delta S°$:

$$\begin{aligned}\ln\sigma &= \ln\left[F\mu_e 2^{1/3} K_{V_O^{2\bullet}}^{1/3}\right] - \frac{1}{6}\ln\left(\frac{P(O_2)}{P^o}\right)\\ &= \ln\left[F\mu_e 2^{1/3}\right] + \left(\frac{\Delta S°_{red\ V_O^{2\bullet}}}{3R}\right) - \left(\frac{\Delta H°_{red\ V_O^{2\bullet}}}{3RT}\right)\\ &\quad - \frac{1}{6}\ln\left(\frac{P(O_2)}{P^o}\right).\end{aligned} \tag{18}$$

The observed slope of − 1 / 6 is characteristic of oxygen vacancy formation (Eq. (13)), showing that below 580 °C Schottky disorder is predominant in TiO_2 Anatase. In this temperature domain (Fig. 6), the activation energy is (1.3 ± 0.1) eV. This value is near those

obtained in air by Azad et al. [20] on porous Anatase ceramics and by Song et al. [11] on microcrystalline Rutile ceramics. The standard enthalpy of reduction can be calculated according to Eq. (18): $\Delta H°_{red\ VO}{}^{2\bullet} = (3.9 \pm 0.3)$ eV. Kofstad [32] and Marucco et al. [10] determined for the Rutile phase: $\Delta H°_{red\ VO}{}^{2\bullet} = 4.6 - 5.0$ eV. Our result is consistent with reduction of TiO_2 at reduced temperature with oxygen vacancy formation. The reduction equilibrium constant $K_{VO}{}^{2\bullet}$ can be obtained from the intercept (corresponding to $P(O_2) = 10^5$ Pa) of the straight line $\log \sigma$ vs. $\log (P(O_2))$ at constant temperature. The electron mobility is assumed to be independent of temperature above 300 K, as in the Rutile phase, and equal to 0.1 $cm^2\ V^{-1}\ s^{-1}$ [33]. This assumption is later justified by the similar electrical behaviour of the two phases. Using the experimental data reported in Fig. 5, we obtain at 557 °C: $K_{VO}{}^{2\bullet}$ (557 °C) = $1.2\ 10^{-30}$. The molar fraction of oxygen vacancies $[V_O{}^{2\bullet}]$ can then be calculated at $P(O_2) = 10^5$ Pa using Eq. (11) and the electroneutrality condition ($n = 2\ [V_O{}^{2\bullet}]$). One obtains: $[V_O{}^{2\bullet}] = (K_{VO}{}^{2\bullet} / 4)^{1/3} = 6.7 \times 10^{-11}$.

4.4. Conductivity data above 650 °C: $\sigma\ \alpha\ P(O_2)^{-1/5}$

In this domain, the conductivity can be written using Eqs. (16) and (17):

$$\begin{aligned} \ln\sigma &= \ln\left[F\mu_e 4^{1/5} K_{Ti_i^{4\bullet}}^{1/5}\right] - \frac{1}{5}\ln\left(\frac{P(O_2)}{P^o}\right) \\ &= \ln\left[F\mu_e 4^{1/5}\right] + \left(\frac{\Delta S°_{red\ Ti_i^{4\bullet}}}{5R}\right) - \left(\frac{\Delta H°_{red\ Ti_i^{4\bullet}}}{5RT}\right) \\ &\quad - \frac{1}{5}\ln\left(\frac{P(O_2)}{P^o}\right). \end{aligned} \tag{19}$$

The slope of − 1 / 5 is characteristic of titanium interstitial formation (Eq. (16)), indicating that at high temperature Frenkel cation disorder is predominant in Anatase. The activation energy determined from the Arrhenius plot (Fig. 6) at higher temperature is (2.2 ± 0.2) eV. Using Eq. (19), we can calculate the standard reduction enthalpy: $\Delta H°_{red\ Ti_i}{}^{4\bullet} = (11 \pm 1)$ eV, consistent with literature data ($\Delta H°_{red\ Ti_i}{}^{4\bullet} = 10.1$ eV [10], [32]). A similar calculation as the previous one using Eq. (19) gives at $P(O_2) = 10^5$ Pa, but higher temperature (T = 700 °C): $K_{Ti_i}{}^{4\bullet}$ (700 °C) = 8.0×10^{-44}. The molar fraction of titanium interstitials is obtained using Eq. (15): $[Ti_i{}^{4\bullet}] = (K_{Ti_i}{}^{4\bullet} / 4^4)^{1/5} = 7.9 \times 10^{-10}$. However, these values were measured at much higher temperature on Rutile, where interstitial formation is observed only above 1100 °C and

under 10^{-1} Pa oxygen pressure. In the case of Anatase, this transition appears already around 600 °C.

The calculated oxygen deficiencies are small, because they correspond to high oxygen partial pressure (pure oxygen). Furthermore, the concentrations of titanium interstitials and oxygen vacancies are quite near and one can imagine that the predominance of one defect type over the other can be tuned by relatively small changes of experimental conditions. A change of majority point defect type is here observed from $V_O^{2\bullet}$ at reduced temperature to $Ti_i^{4\bullet}$ at high temperature. The transition is observed between 600 and 620 °C under 10^{-12} Pa. This behaviour was previously observed by Marucco et al. [10] for Rutile, but at a distinctly higher temperature, between 800 and 1100 °C, around 10^{-12} Pa at 800 °C and around 10^{-1} Pa at 1100 °C. Very recent work by Lee and Yoo [34] on Rutile indicates also that Schottky and Frenkel defect concentrations are very near. The formation of titanium interstitials appears more favourable in Anatase in comparison to Rutile, because Anatase has a 10% lower density than Rutile and the crystal lattice is more open.

Considering the two material reduction Eqs. (10) and (14), one can write:

$$\begin{array}{ll} \left(O_O = V_O^{2\bullet} + 2e' + 1/2\ O_2(g)\right) \times -2 & \Delta H°_{\text{red } V_O^{2\bullet}} \\ Ti_{Ti} + 2\ O_O = Ti_i^{4\bullet} + 4e' + O_2(g) & \Delta H°_{\text{red } Ti_i^{4\bullet}} \\ \hline Ti_{Ti} + 2\ V_O^{2\bullet} = Ti_i^{4\bullet} & \Delta H° = \Delta H°_{\text{red } Ti_i^{4\bullet}} - 2\Delta H°_{\text{red } V_O^{2\bullet}} \end{array}.$$

The calculation gives $\Delta H° = (3.2 \pm 1.6)$ eV, this reaction is endothermic and according to the Le Chatelier's principle, a temperature increase, as well as an increase of the oxygen vacancy concentration, are favourable to the formation of titanium interstitials. This result is in very good agreement with our experimental observations.

Finally, the energy of formation of a point defect may be approximated in the Born model as $z^2e^2/(\varepsilon\varepsilon_0 r_d)$ where z is the charge number, e the electronic charge, $\varepsilon\varepsilon_0$ the permittivity of the solid and r_d is the defect radius [35]. Considering only the charge numbers (i.e. ignoring the difference in radius between an oxygen vacancy $V_O^{2\bullet}$ and a titanium interstitial $Ti_i^{4\bullet}$), the energy of formation of an interstitial titanium is approximately four times that of an oxygen vacancy ($z^2 = 2 \times 2$ versus 4×4, respectively). This qualitative argument for an easier creation of oxygen vacancies is in good agreement with the experiment.

5. Conclusion

The electrical conductivity of dense Anatase TiO_2 ceramics is investigated. The oxygen partial pressure and temperature dependence show clearly a change from predominant Schottky disorder at low temperature and high $P(O_2)$ to predominant cation Frenkel disorder at high temperature and low $P(O_2)$. Simple thermodynamic arguments for this observation are given.

Acknowledgments

The authors thank Dr. A. Garnier (MADIREL) for the XRD measurements and Dr. W. Saikaly (CP2M) for help in the TEM investigations.

References

R.M. Alberici, M.C. Canela, M.N. Eberlin and W.F. Jardim, *Appl. Catal., B* 30 (2001), p. 389.

Ch.J. Barbe, F. Arendse, P. Comte, M. Jirousek, F. Lenzmann, V. Shklover and M. Grätzel, *J. Am. Ceram. Soc.* 80 (1997), p. 3157.

W. Büchner, R. Schliebs, G. Winter and K.-H. Büchel, Industrial Inorganic Chemistry, VCH, Weinheim (1989), p. 526.

M.R. Ranade, A. Navrotsky, H.Z. Zhang, J.F. Banfield, S.H. Elder, A. Zaban, P.H. Borse, S.K. Kulkarni, G.S. Doran and H.J. Whitfield, *PNAS* 99 (2002), p. 6476.

J. Nowotny, M. Radecka, M. Rekas, S. Sugihara, E.R. Vance and W. Weppner, *Ceram. Int.* 24 (1998), p. 571.

P. Kofstad, Nonstoichiometry, Diffusion and Electrical Conductivity in Binary Metal Oxides, Wiley Interscience Publication, New York (1972), p. 145.

R.N. Blumenthal, J. Baukus and W.M. Hirte, *J. Electrochem. Soc.* 114 (1967), p. 172.

K. Hauffe, J. Hupfeld and T. Wetterling, *Z. Phys. Chem.* 103 (1976), p. 115.

H.P.R. Frederikse, *J. Appl. Phys.* 32 (1961), p. 2211.

J.F. Marucco, J. Gautron and P. Lemasson, *J. Phys. Chem. Solids* 42 (1981), p. 363.

S.H. Song, X. Wang and P. Xiao, *Mater. Sci. Eng., B* 94 (2002), p. 40.

C. Demetry and X. Shi, *Solid State Ionics* 118 (1999), p. 271.

H. L. Tuller, personal communication.

J.F. Baumard and E. Tani, *Phys. Status Solidi, A* 39 (1977), p. 373.

J.L. Carpentier, A. Lebrun, F. Perdu and P. Tellier, *C.R. Acad. Sc., Paris, série II* vol. 304 (1987), p. 1489.

D.C. Cronemeyer, *Phys. Rev.* 87 (1952), p. 876.

V.P. Popov, V.E. Svaiko-Svaikovski and A.A. Andreev, *Fiz. Tverd. Tiela (Russ Solid State Phys.)* 21 (1979), p. 383.

L. Singheiser and W. Auer, *Ber. Bunsenges. Phys. Chem.* 81 (1977), p. 1167.

P. Knauth and H.L. Tuller, *J. Appl. Phys.* 85 (1999), p. 897.

A.M. Azad, S.A. Akbar and L.B. Younkman, *J. Am. Ceram. Soc.* 77 (1994), p. 3145.

S. Bhowmik, K.P. Constant, J.C. Parker and M. Ali, *Mater. Sci. Eng., A* 204 (1985), p. 258.

C. Cantalini and M. Pelino, *J. Am. Ceram. Soc.* 75 (1992), p. 546.

P. Knauth, R. Bouchet, O. Schäf, A. Weibel and G. Auer, Synthesis, Functionalization and Surface Treatments of Nanoparticles. In: M.-I. Baraton, Editor, American Science Publ, Stevenson (2002).

A. Weibel, R. Bouchet, F. Boulc'h and P. Knauth, *Chem. Mater.* 17 (2005), p. 2378.

A. Weibel, R. Bouchet and P. Knauth In: P. Knauth, J.-M. Tarascon, E. Traversa and L. Tuller, Editors, *Materials Research Society Symposium Proceedings* vol. 756 (2003), p. 193 Warrendale.

J. Fouletier, P. Fabry and M. Kleitz, *J. Electrochem. Soc.* 123 (1976), p. 204.

M.C. Steil, Thesis, Université Joseph Fourier, Grenoble (1996).

J. Fouletier, E. Siebert and A. Caneiro, *Adv. Ceram.* 12 (1984), p. 618.

F.A. Kröger, The Chemistry of Imperfect Crystals (2nd edition), Holland Publishing Company, Amsterdam (1974), p. 2.

K.M. Reddy, S.V. Manorama and A.R. Reddy, *Mater. Chem. Phys.* 78 (2002), p. 239.

J.F. Marucco, J. Gautron, P. Lemasson and J.P. Loup, *C.R. Acad. Sci. Paris* 289C (1979), p. 117.

P. Kofstad, Nonstoichiometry, Diffusion and Electrical Conductivity in Binary Metal Oxides, Wiley Interscience Publication, New York (1972), p. 142.

T. Bak, J. Nowotny, M. Rekas and C.C. Sorrell, *J. Phys. Chem. Solids* 64 (2003), p. 1069.

D.-K. Lee, H.-I. Yoo, Solid State Ion. (in press).

K. Ismail, E. Sikora and D.D. Macdonald, *J. Electrochem. Soc.* 145 (1998), p. 3141.

Original text : Elsevier.com